nature communications

Article

https://doi.org/10.1038/s41467-025-60117-5

Engineered microbial platform confers resistance against heavy metals via phosphomelanin biosynthesis

Received: 9 August 2024

Accepted: 15 May 2025

Published online: 24 May 2025

Check for updates

Xiaokang Ren[1,2,4], Luyang Zhao[1,4], Jintao Shen[1], Peng Zhou[1], Kaili Zhao[1,2], Chengqian Yuan[1], Ruirui Xing[1,2] ✉ & Xuehai Yan[1,2,3] ✉

Environmental concerns are increasingly fueling interest in engineered living materials derived from microbial sources. Melanin biosynthesis in microbes, particularly facilitated by recombinant tyrosinase expression, offers sustainable protection for the habitat of microorganisms against severe environmental stressors. However, there exists a vast urgency to optimize these engineered microbial platforms, which will amplify their protective capabilities, integrate multifaceted functions, and thereby expand their utility and effectiveness. Here, we genetically engineer microbial platforms capable of endogenously biosynthesizing phosphomelanin, a unique phosphorus-containing melanin. The ability to heterogeneously biosynthesize phosphomelanin endows the microbes with enhanced resistance to heavy metals, thus safeguarding their survival in adverse conditions. Furthermore, we upgrade these engineered microbes by integrating PET-degrading enzymes, thereby achieving effective integrated management of metallized plastic waste. This engineered microbial platform, with its phosphomelanin biosynthetic capabilities, presents significant opportunities for microbes to engage in bioengineering manufacturing, potentially serving as the next-generation guardians against global ecological challenges.

Heavy metals (HMs) and metallized wastes constitute a persistent and pervasive global environmental challenge[1,2]. HMs are a collection of metallic elements characterized by their high density, and toxicity or harmfulness to living organisms[3]. Being non-biodegradable, they have a tendency to bio-accumulate in the tissues of organisms and undergo bio-magnification across trophic levels. This process can lead to detrimental health effects across the spectrum of life forms, including microbes, plants, animals, and humans. Various strategies have been developed for the remediation of HM pollution. The most commonly used method involves the addition of amendments such as precipitating chelating agents (e.g., limestone, lime)[4], complexing chelating agents (e.g., ethylenediaminetetraacetic acid, citric acid)[5], and phosphate compounds[6]. These amendments can help immobilize HMs, reducing their bioavailability and mobility, and thereby decreasing their toxicity. However, conventional methods for HM removal have several drawbacks, including potential secondary pollution risks and significant alterations to the physical and chemical properties of soil and water[7]. Consequently, it is imperative to explore efficient and cost-effective methods to mitigate the ecological damage caused by HMs and metallized wastes, while also minimizing the associated risks to human health during the remediation process.

Microbes play a multitude of vital roles in environmental protection, including the purification of pollutants and the bio-remediation of contaminated sites, thereby contributing to the sustainability and resilience of ecosystems[8–10]. Microbial biotechnology has thus emerged as an effective and eco-friendly solution for the treatment of HMs and

[1]State Key Laboratory of Biopharmaceutical Preparation and Delivery, Institute of Process Engineering, Chinese Academy of Sciences, Beijing 100190, China. [2]University of Chinese Academy of Sciences, Beijing 100049, China. [3]Center for Mesoscience, Institute of Process Engineering, Chinese Academy of Sciences, Beijing 100190, China. [4]These authors contributed equally: Xiaokang Ren, Luyang Zhao. ✉e-mail: rrxing@ipe.ac.cn; yanxh@ipe.ac.cn

metallized waste[11]. It is well known that metals are involved in the growth and metabolism of microbes in the process of their adaptive evolution, either directly or indirectly[12]. Precisely for this reason, microbes can exhibit resistance to HMs. However, exposure to high levels of HMs can cause irreversible damage to microbes. This includes the disruption of microbial structures, disturbance of oxidative phosphorylation, conformational alterations of nucleic acids and proteins, and the induction of enzyme inactivation[13]. Enhancing the resistance to HMs is crucial for improving the effectiveness of microbes as a sustainable and efficient approach for HM pollution management.

Melanogenic microbes, leveraging their inherent metal tolerance mechanisms and the endogenous biosynthesis of melanin, demonstrate metallophilic and metal-resistant characteristics superior to those of ordinary microbes[14]. This renders them highly effective for the bio-remediation of HM-polluted environments, due to the metal affinity and high adsorption capacity of melanin. A typical example is *A. salmonicida* subsp. *pectinolytica*, an extremophile isolated from a heavily polluted river, which utilizes its own oxidase and peroxides to manipulate the cascade biosynthesis of melanin[15]. The melanin biosynthesized within this extremophile acts as metal-binding agents, providing protection against high concentrations of HMs[16]. Additionally, the Gram-positive bacterium *Bacillus megaterium* (*B. megaterium*) is a versatile and stress-resistant melanogenic bacterium capable of resisting HMs[17,18]. While melanogenic microbes provide a sustainable and eco-friendly alternative for HM removal, the low concentrations of melanin generated by naturally-occurring strains are currently insufficient to address the escalating issue of HM contamination[10].

Engineering microbial systems aim to customize or optimize microbes with programmable functionalities using genetically engineered and approaches. This nascent field holds the potential to revolutionize diverse sectors, from sustainable manufacturing to environmental management and ecological sustainability[19]. Currently, ongoing efforts are focused on the overexpression of genes responsible for melanin-producing enzymes (eg., tyrosinases (TYRs), phenoloxidases) in both melanogenic and non-melanogenic microbes, have not only boosted the inherent melanogenic potential, but also enabled the creation of melanin-recombinant microbial strains[20,21]. Nowadays, engineered microbes have successfully facilitated the endogenous synthesis of several melanins. However, most of reported works on microbial melanin production have focused on eumelanin and its analogs[14,22]. This is highly acceptable, as eumelanin is the most common type of melanin in humans. The melanins produced by engineered microbes currently face issues such as poor yield, low purity, unsatisfactory bioactivity and limited functionality. The currently known melanins, such as eumelanin, pheomelanin and artificial melanin analogs, possess similar polymeric backbones and functional groups (eg., catechol, quinone), which represent only a small fraction of their chemical diversity[21–24]. By developing new types of melanin, we can explore more undiscovered or underutilized chemical structures, thereby developing engineered microbes with optimized HMs binding performance and broadened application scope. Engineering microbial systems holds the potential to revolutionize diverse sectors, from sustainable manufacturing to environmental management and ecological sustainability. However, there is considerable scope for further progress in the engineering of microbes capable of biosynthesizing melanins to combat HM pollution.

The phosphate group, a key component of essential biomolecules such as nucleic acids and adenosine triphosphate (ATP), has a strong tendency to interact with metal ions[25,26]. For instance, metachromatic granules are densely packed particles widely found within bacteria, the main component of which is polyphosphate (polyP), and play a significant role in microbial resistance to environmental HM stress. At the same time, most chassis microorganisms are capable of utilizing organophosphorus compounds and converting them into endogenous substances[18]. The current technological system still faces limitations due to its reliance on exogenous substrate supply, which constrains the practical application of phosphomelanin biosynthesis in comprehensive HM pollution remediation. Therefore, we look forward to develop a de novo biosynthesis strategy for phosphomelanin through engineered chassis microorganisms, aiming to establish an autonomous production platform in future.

In this work, we design and engineer a melanogenic microbial platform capable of biosynthesizing of phosphorus-enriched melanin, designated as phosphomelanin. By employing chassis organisms with upregulated tyrosinase (TYR) gene expression and using a phosphorylated tripeptide substrate, we demonstrate that peptide-based substrates enable customized enzymatic reactions due to their structural flexibility and tunability[27–29]. This approach generates microbial systems with programmable properties capable of endogenous phosphomelanin production. Further, we demonstrate here that the production of phosphomelanin endows the microbes with enhanced resistance to HMs. Moreover, we showcase the potential of combining phosphomelanin biosynthesis with the functionality of poly (ethylene terephthalate) degrading enzymes (PETase) within an engineered melanogenic microbial platform, thereby achieving effective and integrated management of metallized plastic waste.

Results

Phosphomelanin production from engineered melanogenic microbes

TYR functions as a prototypical multifunctional binuclear copper oxidase pivotal in melanogenesis and enzymatic browning processes[30]. The manipulation of the TYR gene, which is essential for melanin and its analogues production in living organisms, enables the customization of microbes to achieve enhanced TYR expression. In our work, we selected *B. megaterium* (WH320) as the microbial chassis. Using a standard genome editing method[31], we successfully developed an engineered bacterium (GE-WH320) with effective expression of the TYR gene (Fig. 1a-c and Supplementary Fig. 1). Initially, we engineered a shuttle plasmid, designated as phis 1525, which incorporated the promoter and repressor genes of the *B. megaterium*-borne xylose utilization operon. The TYR gene from bacteria (referred to as the bmTYR gene) was then integrated into phis 1525 under the control of the xylose operon, resulting in the recombinant shuttle plasmid phis1525-bmTYR. After transforming phis 1525-bmTYR into WH320, we obtained the engineered bacterium (GE-WH320).

TYR features a spacious active site pocket that is specifically tailored to accommodate Tyr-based substrates, thereby facilitating their conversion into melanin or melanin analogues[32–35]. In our study, we designed the tripeptide Ser-Tyr-Gly (SYG) and the phosphorylated tripeptide $_{p}$Ser-Tyr-Gly ($_{p}$SYG) as substrates. The SYG is derived from the reactive sequence found in the green fluorescence proteins of *Aequorea victoria*[36], wherein Tyr functions as the site for the enzyme-catalyzed reaction, and Ser provides a covalent bonding site for the phosphate group, thereby facilitating the efficient phosphorylation of melanin and its analogues. The molecular structures of these two tripeptides were subsequently elucidated using a combination of nuclear magnetic resonance (NMR) and high-resolution electrospray ionization mass spectroscopy (ESI-MS) (Supplementary Figs. 2 and 3). Following a 12-hour co-culturing of the GE-WH320 with $_{p}$SYG, a macroscopic colonial browning reaction was evident in the culture medium. This pronounced color change was not detected during the co-incubation of the WH320 with $_{p}$SYG (Fig. 1d and Supplementary Fig. 4a). The observed coloration suggests that the engineered bacteria are highly expressing the TYR, which catalyzes the Tyr-containing tripeptide substrate to produce melanin analogues[33]. Scanning electron microscopy (SEM) revealed the generation of heterogeneous aggregates within the GE-WH320 following co-culturing with $_{p}$SYG. This resulted in a transition from smooth to rough bacterial surfaces, attributable to the deposition of these melanin analogues (Fig. 1e). The

https://doi.org/10.1038/s41467-025-60117-5

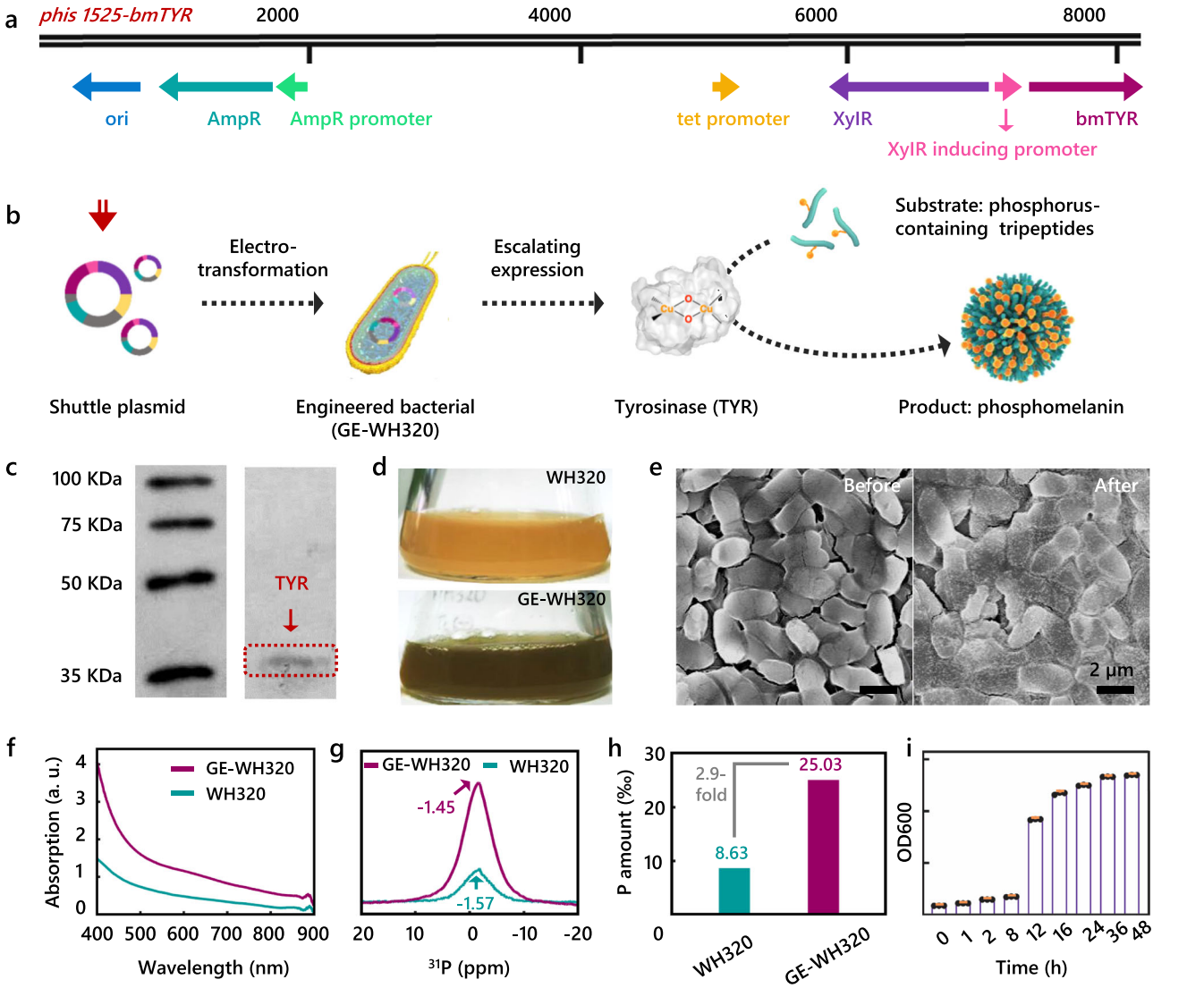

Fig. 1 | Phosphomelanin production from engineered bacteria. a The physical map of the recombinant shuttle plasmid 1525-bmTYR. **b** Schematic representation of the biosynthesis of phosphomelanin in engineered bacteria. The expressed TYR catalyzed substrate (phosphorylated tripeptide, $_{p}$SYG) to produce phosphomelanin eventually. **c** WB analysis of GE-WH320 confirmed the expression of bmTYR, with a molecular weight of 38.1 kDa. **d** Image of culture mediums of GE-WH320 and WH320 bacteria after incubation with $_{p}$SYG over 72 h, show a distinct color difference. **e** SEM images of GE-WH320 before and after a 72-hour incubation with $_{p}$SYG. **f** UV-vis absorption spectra of GE-WH320 and WH320 bacteria after 72-hour incubation with $_{p}$SYG. **g** The ^{31}P ssNMR spectra of bacteria, indicate a stronger phosphorus signal intensity in the GE-WH320 compared to the WH320 bacteria at the same conditions. **h** The ICP-OES results of these two bacteria, showing that the phosphorus amount in GE-WH320 increased 2.9-fold to WH320 bacteria (25.03‰ vs. 8.63‰). **i** The average optical density at 600 nm (OD_{600}) of the culture medium changes over time, indicating the generation of phosphomelanin within bacteria does not affect their growth and proliferation ($n = 3$). Source data are provided as a Source Data file.

co-incubation melanin analogues derived from the GE-WH320 exhibited amplified absorption in the UV-vis region when compared to those from the WH320 (Fig. 1f). These observations collectively validate the successful biosynthesis of brown-black pigments within the engineered bacteria, which possess classic characteristics of melanin.

Co-culturing with phosphorylated substrates resulted in a notably amplified phosphorus signal intensity in the GE-WH320 compared to WH320, as evidenced by ^{31}P solid-state NMR (ssNMR) spectroscopy (Fig. 1g). Furthermore, inductively coupled plasma optical emission spectrometry (ICP-OES) was employed for the quantitative analysis of phosphorus content within these bacterial samples. The results indicated that when $_{p}$SYG was used as the substrate, the phosphorus content in GE-WH320 increased significantly, by 2.9 times compared to that in WH320 bacteria. Additionally, the analysis revealed that the phosphorus content in GE-WH320 with $_{p}$SYG as the substrate was significantly increased by 3.19 times, compared to that with SYG as the substrate (Fig. 1h and Supplementary Fig. 5). These results underscore an augmented accumulation of phosphorus during the biosynthesis process of melanin analogues catalyzed by TYR within the engineered bacteria. These findings signify the successful biosynthesis of a phosphorus-containing melanin analogue, which we have designated as phosphomelanin, within the customized engineered bacteria. The intracellular enzymatic cascade oxidation process involving phosphorus, as the critical step in the biosynthesis of phosphomelanin, is found to be an exceedingly mild procedure. SEM results unveiled that the cell wall and cytoplasmic membrane of the engineered bacteria retained their structural integrity subsequent to phosphomelanin generation. After transferring these colonies that have generated phosphomelanin to fresh Luria-Broth (LB) medium, they were able to undergo successive divisions and exhibited exponential growth according to the S-shaped growth curve[37] (Fig. 1i and Supplementary Fig. 4b, c).

Structural analysis of phosphomelanin

The commercially available TYR extracted from the champignon mushroom *Agaricus bisporus* (referred to as abTYR) exhibits high homology with bmTYR (Supplementary Fig. 6a), attributable to their shared dicopper active centers[30]. To assess the similarity between bmTYR and abTYR, equivalent amount of the phosphorylated substrates $_{p}$SYG, $_{p}$TYG, and $_{p}$YYG were co-incubated with both TYRs at 37 °C for 48 h under aerobic conditions. UV-vis absorption spectra confirmed similar patterns of melanin analog generation and accumulation in vitro (Supplementary Fig. 6b). Moreover, the ^{31}P ssNMR spectroscopic features of the phosphomelanin catalyzed by abTYR are consistent with those of the phosphomelanin generated by bmTYR (Supplementary Fig. 6c). This makes abTYR a well-suited model for in vitro studies of melanogenesis. Notably, when compared to the substrate $_{p}$SYG, the phosphomelanin ($_{p}$SYG$_{ox}$) exhibited resonance peaks with comparable ^{31}P chemical shifts (δ), signifying a high degree of consistency in their chemical structure[33]. This suggests that the $_{p}$SYG$_{ox}$ is synthesized through the polymerization of the substrate peptide molecules ($_{p}$SYG). The generated $_{p}$SYG$_{ox}$ was verified as a water-soluble, heterogeneous aggregate with a black, electron-dense structure, as revealed by cryo-transmission electron microscopy (cryo-TEM) (Supplementary Fig. 7). The in vitro synthesis of $_{p}$SYG$_{ox}$ via abTYR-catalyzed oxidative polymerization achieved a high yield rate of 57% after 48 h.

Leveraging a combination of ^{13}C NMR and ^{13}C ssNMR techniques, we unraveled the abTYR-catalyzed oxidative polymerization process responsible for the formation of $_{p}$SYG$_{ox}$. In the ^{13}C NMR spectra, signals at positions 1/1′ (δ = 130 ppm) and 2/2′ (δ = 115 ppm), corresponding to the *meta*- and *ortho*-carbons of the hydroxyl carbon within the aromatic region[38], demonstrated a strong consistency between the structure of substrates ($_{p}$SYG) and its oxidized products ($_{p}$SYG$_{ox}$). This consistency served as evidence of the generation of polymers with repeating units (Fig. 2a). Moreover, the intensities of these two signals assigned to *meta*-carbon and *ortho*-carbon were notably augmented in the cross-polarization/magic angle spinning (CP/MAS) ^{13}C ssNMR spectrum compared to those detected by ^{13}C NMR (Fig. 2b). This observation indicated that the abTYR-catalyzed oxidative polymerization on the phenolic hydroxyl group in the substrate monomer $_{p}$SYG resulted in the formation of densely packed solid-state structures[39]. Furthermore, matrix-assisted laser desorption/ionization time of flight mass spectrometry (MALDI-TOF-MS) provided additional evidence for the polymeric structure of $_{p}$SYG$_{ox}$ (Supplementary Fig. 8), revealing characteristic structurally heterogeneous and multi-dispersed oligomeric fragments. The Fourier Transform Infrared (FTIR) spectrum of the substrate $_{p}$SYG revealed the presence of phenolic groups from Tyr, as evidenced by the distinct absorbance band at 1518 cm^{-1} [40]. Following abTYR-catalyzed oxidative polymerization, the FTIR spectrum of $_{p}$SYG$_{ox}$ showed the disappearance of the 1518 cm^{-1} band and the emergence of a characteristic band at 1601 cm^{-1}, which corresponds to quinone moieties (Fig. 2c). These findings conclusively demonstrate that the enzymatic polymerization process of phosphomelanin involves a phenol-to-quinone oxidative reaction. Notably, this phenol-to-quinone transition can also be observed in the substrate SYG (Supplementary Fig. 9).

The chemical forms of phosphorus within $_{p}$SYG$_{ox}$ were further elucidated using ^{31}P NMR spectroscopy. For the substrate $_{p}$SYG, its ^{31}P NMR spectrum featured a distinct and narrow peak signal at 3 (δ = −0.32 ppm), corresponding to the phosphate group on the Ser residue. This chemical form was also detected in $_{p}$SYG$_{ox}$ (3′, δ = 0.76 ppm). Additionally, a peak signal at 4 (δ = 2.6 ppm) emerged for $_{p}$SYG$_{ox}$, indicating the existence of a newly generated chemical form of phosphorus, which may be a phosphate diester (Fig. 2d). These above two chemical forms of phosphorus were also detectable through ^{31}P ssNMR, with corresponding peak signals at δ = −0.98 ppm and δ = 2.04 ppm, respectively (Supplementary Fig. 10). A comparative analysis of the ^{13}C NMR spectra for SYG$_{ox}$ and $_{p}$SYG$_{ox}$ provided further insight into the newly generated chemical form of phosphorus. In SYG$_{ox}$, a single sharp peak was observed at δ = 176.3 ppm, which was assigned to the *o*-quinone groups of oxidized Tyr (Supplementary Fig. 11a). In comparison, $_{p}$SYGox exhibited two peaks in the aromatic region of δ = 176.3 and 175.2 ppm (Supplementary Fig. 11b), with the former peak not being observed in SYG$_{ox}$. The unique signal at δ = 175.2 ppm is attributed to the quinone structure attached to a newly formed phosphate group[41–43]. The above results confirm that phosphorus in $_{p}$SYG$_{ox}$ exists in the form of a phosphoester bond (R-H_2PO_4), most likely coexisting in two chemical forms: one is the intrinsic phosphate monoester retained from the substrates ($_{p}$SYG), and the other is a newly generated phosphate diester that bridges both Ser and the quinone group of oxidized Tyr via P-O-C chemical bonds (Supplementary Fig. 12).

The process of phosphomelanin generation through abTYR-catalyzed oxidative polymerization can be speculated as follows (Fig. 2e). In Stage I, a sequential cascade of oxidation catalysis was initiated, commencing from *mono*-phenol and proceeding to *di*-phenol, and ultimately leading to the formation of the quinone intermediate. Advancing to Stage II, the essential repetitive building blocks of phosphomelanin were formed, involving the phosphoester bond-forming reaction. Subsequently, in Stage III, the oxidative polymerization process continued, leading to the elongation and diversification of the polymer chains, ultimately yielding the heterogeneous phosphomelanin. The abTYR directly participates in the three-stage enzymatic oxidation process, ultimately driving the biosynthesis of phosphomelanin[34,35]. In natural systems, there are several classical types of protein phosphorylation that play essential roles in cellular signaling and regulation[44]. These types, apart from Ser phosphorylation, typically include Thr phosphorylation and Tyr phosphorylation. In our study, we further purposefully designed and synthesized phosphate-containing tripeptides including $_{p}$Thr-Tyr-Gly ($_{p}$TYG) and $_{p}$Tyr-Tyr-Gly ($_{p}$YYG) (Supplementary Figs. 13-14), to simplify mimic the phosphorylated proteins found in nature. Co-incubation of these two substrates with abTYR can also resulted in generation of phosphomelanin (Supplementary Figs. 15 and 16). The experimental results obtained from the UV-vis absorption spectra, ^{31}P NMR spectra, and ^{13}C NMR spectra provided evidence that, in the presence of abTYR, the substrate molecules underwent oxidative polymerization, resulting in the formation of phosphomelanin ($_{p}$TYG$_{ox}$ and $_{p}$YYG$_{ox}$). Given the important role of phosphorylation in organisms, elucidating the biosynthesis of phosphomelanin will offer new insights into the evolution of melanin function and the genetic foundation of melanization in microorganisms[45].

Kinetics of enzymatic production of phosphomelanin

TYR is composed of a four-helix bundle core bearing a magnetically coupled dinuclear copper center in a deep active site pocket, capable of oxidizing phenols attached to cargo molecules to yield *o*-quinones[30]. These copper ions facilitate the transfer of an atom from molecular oxygen (O_2) to the orthoposition of a bound phenol molecule. With the aim to elucidate the nature of the copper binding sites and the presence of radical intermediates of the copper ions in abTYR, spectroscopic studies by EPR were carried out. Results revealed the existence of an EPR-silent state around g = 2.50 ~ 2.05 (Supplementary Fig. 17a). The absence of the EPR signal has been shown to derive from antiferromagnetic coupling between the copper (II)s, which requires a super exchange pathway associated with a bridging ligand[30].

The kinetics of abTYR-catalyzed oxidative polymerization of phosphomelanin can be elucidated based on three historically recognized states of the active center copper atom: *deoxy* [Cu(I)-Cu(I)]; *oxy* [Cu(II)-O_2^{2-}-Cu(II), μ-η^2:η^2-peroxido dicopper (II)]; and *met* [Cu(II)-O-Cu(II), μ-hydroxido dicopper (II)][34,46]. In the initial stage of phosphomelanin biosynthesis, the abTYR in the *deoxy*-form state activates O_2 to

https://doi.org/10.1038/s41467-025-60117-5

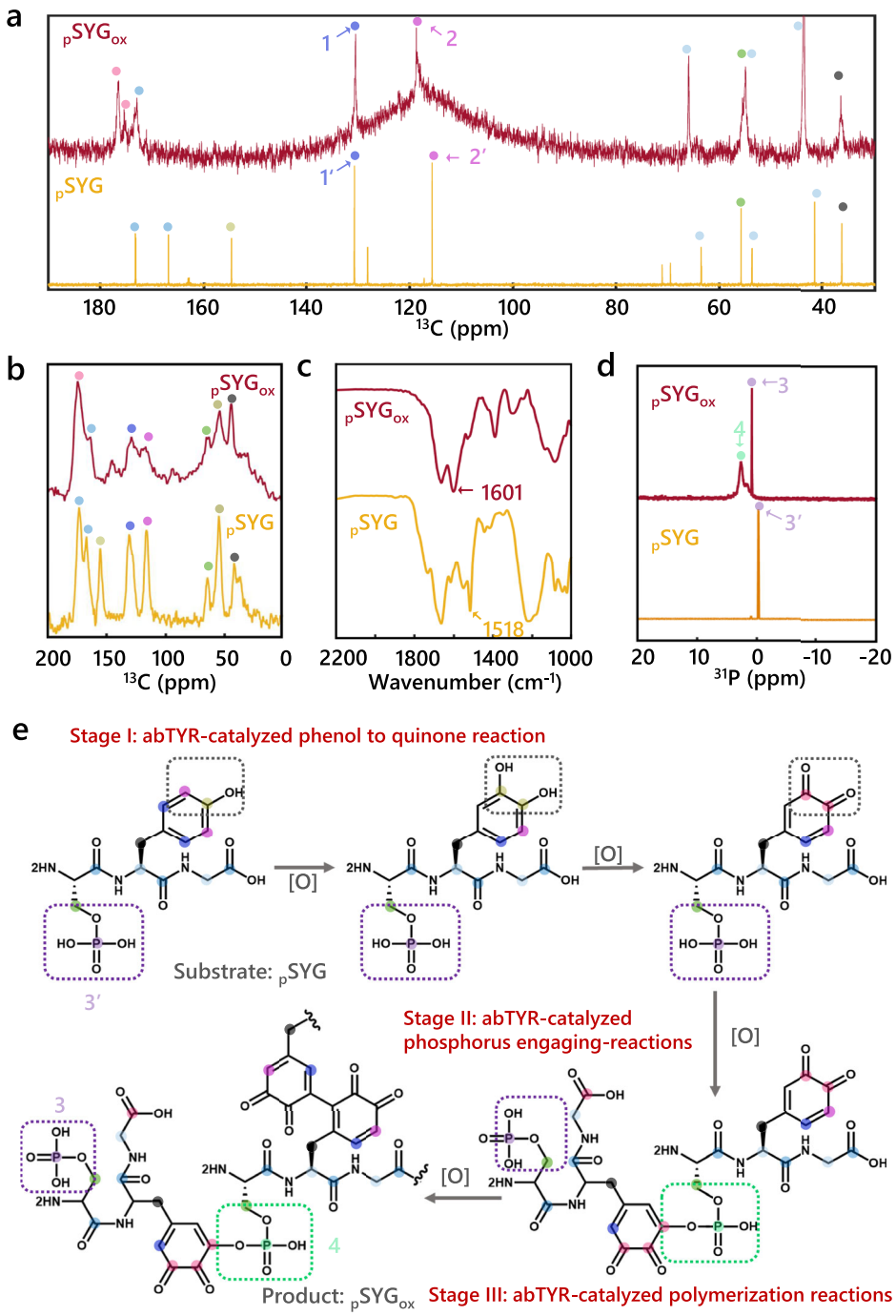

Fig. 2 | Structural characterizations of phosphomelanin. a ^{13}C solution-state NMR spectra of $_pSYG$ and $_pSYG_{ox}$, signals corresponding to the whole molecular backbones were detected, attributed and remarked by different color dots. **b** ^{13}C CP/MAS ssNMR spectra of $_pSYG$ and $_pSYG_{ox}$. **c** FTIR spectra of $_pSYG$ and $_pSYG_{ox}$. These bands located at 1601 cm^{-1} was attributed to quinone residues. The band located at 1518 cm^{-1} was ascribed to phenol groups of Tyr. **d** ^{31}P solution-state NMR spectra of $_pSYG$ and $_pSYG_{ox}$, a new resonance of $_pSYG_{ox}$ indicated a newly generated chemical form of phosphorus was synthesized during enzymatic reactions. **e** The underlying mechanism of the biosynthesis of phosphomelanin by abTYR. Three stages can be divided based on the proposal structures. Stage I is the classical oxidative reactions of phenol groups to produce quinone groups. Stage II was the P-O-C bond-forming reaction to introduce a phosphate group, and Stage III was the polymerization reaction between these aromatic (phenol or quinone) groups to produce the heterogenous pigmental polymer. Source data are provided as a Source Data file.

generate a μ-η^2:η^2-peroxido dicopper (II) core, representing the *oxy*-form state. This leads to the regioselective hydroxylation of phenols, resulting in the formation of catechols, while concurrently forming a μ-hydroxido dicopper (II) core (*met*-form state). Subsequently, abTYR facilitates the further oxidation of catechols to quinones, while the copper core in the *met*-form state reverts back to the *deoxy*-form state (Supplementary Fig. 18a). Kinetic experiments using $_pSYG$ and SYG as substrates respectively, were performed by monitoring spectrophotometrically the corresponding melanin analogues in the region of 300 ~ 800 nm. Results showed that under the commensurate enzyme-catalyzed reaction conditions, phosphorus-containing substrates ($_pSYG$) exhibit higher enzymatic reaction efficiency compared to substrates without phosphorus (SYG) (Supplementary Figs. 17b and 18b-c). In addition to the pathway in which TYR catalyzes the oxidative polymerization of Tyr residues resulting in the production of melanin, a parallel competitive pathway exists. This pathway involves

TYR catalyzing the oxidative cross-linking of Tyr residues to form stable and covalent *o, o'*-dityrosine products with characteristic fluorescence. Excitation of those fluorescent intermediates at a wavelength of 315 nm results in a characteristic emission centered on 400 nm[35]. It was observed that the fluorescence generated in the abTYR-catalyzed process using $_{p}$SYG as the substrate was significantly lower than that using SYG as the substrate (Supplementary Figs. 18d-e and 19). These results indicated that the introduction of phosphorus in the substrates can significantly enhance the efficiency of abTYR in catalyzing the oxidative polymerization, thereby leading to improved melanin production.

Further, energy analysis and molecular docking studies were conducted to reveal the influence of phosphorus-containing groups on the abTYR-catalyzed oxidative reactions. In the simulation, the subunit of recombinant mushroom TYR (abPPO4, PDB ID: 5M6B, chain A) was taken as the receptor, and substrates including $_{p}$SYG and SYG were used as ligands[47]. The computational docking results were visualized to illustrate the strength of the bonding forces and the best geometrical arrangements of the substrate molecule ($_{p}$SYG and SYG) within the active pocket of the abPPO4 enzyme (Supplementary Fig. 17c-d). Results showed that phosphorus-containing groups in substrates $_{p}$SYG provided abundant hydrogen bonding sites inside TYR (abPPO4) enzyme. Amino acid residues Cys80, Ser83, Lys421, and Thr457 formed six hydrogen bonds with $_{p}$SYG. Comparably, only two hydrogen bonds located on the Cys80 and Thr457 were found between this enzyme and SYG. The predicted binding energy for $_{p}$SYG is −2.7 kcal mol^{-1}, which is stronger than that for SYG at −2.4 kcal mol^{-1}. Consequently, it can be concluded that $_{p}$SYG demonstrates a higher binding affinity to abTYR than SYG, implying that phosphorus-containing substrates may enhance the activity of abTYR-catalyzed oxidative reactions.

Metal binding ability of phosphomelanin

Given the bioaccumulation, persistence, and toxicity of HMs, there is an urgent need for sustainable remediation approaches to address their environmental hazards[3]. Melanin have the ability to form stable complexes with HMs through various functional groups, such as hydroxyl, carboxyl, and phenolic hydroxyl[48]. Building on this eco-friendly strategy, we have investigated the metal adsorption and removal capabilities of phosphomelanin with a focus on its interactions with a selection of representative HMs, including Cr^{II}, Pb^{II}, Yb^{III}, Dy^{III}, and Tb^{III} (Fig. 3a). Upon mixing the nitrate salts of the aforementioned HMs with $_{p}SYG_{ox}$ in aqueous solutions, the initially tawny-colored $_{p}SYG_{ox}$ solution lightened to a pale yellow (for Cr^{II}) and became colorless (for Pb^{II}, Yb^{III}, Dy^{III}, and Tb^{III}). Concurrently, insoluble dark-colored complexes rapidly formed and precipitated (Fig. 3b). The findings indicate that phosphomelanin forms effective complexes with HMs, transforming them into easily manageable precipitates, and surpasses traditional melanin in sequestration capabilities. The strong binding capabilities of phosphomelanin with HMs was also supported by the results from UV-vis spectroscopy (Fig. 3c) and ICP-OES (Fig. 3d and Supplementary Fig. 20). Under identical conditions, the incorporation of phosphorus significantly enhanced the melanin's ability to remove Cr^{II}, Pb^{II}, Yb^{III}, Dy^{III}, and Tb^{III}, with the concentrations of HMs in the precipitates increasing by 41.80%, 4.01%, 32.18%, 51.70%, and 8.67%, respectively.

Subsequently, we employed a suite of ssNMR techniques, including 1D ^{1}H NMR spectra, 1D ^{31}P NMR spectra, as well as 2D ^{1}H-^{31}P heteronuclear chemical shift correlation experiments (HETCOR) under magic angle spinning (MAS), to elucidate the intermolecular interactions within HM-phosphomelanin complexes. These analyses were instrumental in revealing the mechanisms by which phosphorus-containing melanin augment the binding capacity for HMs. Specifically, we selected the Pb^{II}-$_{p}SYG_{ox}$ complex as an example to provide insights into the role of phosphorus-containing moieties in the sequestration of HMs. As shown in Fig. 3e, f, the 1D ^{31}P and ^{1}H NMR spectra were utilized to investigate the alterations in electron density of the Pb^{II}-bound and Pb^{II}-free states of $_{p}SYG_{ox}$. After the formation of the Pb^{II}-$_{p}SYG_{ox}$ complex, the ^{31}P resonance shifted to a higher field region. This indicated that Pb^{II} caused a change in the electron density around the phosphorus atom. This can be attributed to the electrostatic interaction between the negatively charged phosphorus groups and the positively charged Pb^{II}. And, the ^{1}H resonances indicated that the aromatic hydrogen ($H_{aromatic}$) and the active hydrogen (H_{active}) in Pb^{II}-$_{p}SYG_{ox}$ complex all shifted to a higher field region, while the resonance of aliphatic hydrogen ($H_{aliphatic}$) stayed the same. These results above indicate that Pb^{II} interacts with the carboxyl, dopaquinone, and phosphoryl groups of $_{p}SYG_{ox}$, facilitating the adsorption and removal of HMs by the phosphomelanin. Furthermore, 2D ^{1}H-^{31}P HETCOR spectra were measured to provide more detailed structural information of Pb^{II}-$_{p}SYG_{ox}$ complex[49,50]. Two groups of ^{31}P resonances were detected from $_{p}SYG_{ox}$, which correspond to different phosphate groups (around −0.94 and 0.23 ppm), respectively (Fig. 3g, Supplementary Table 1). Upon complexation with Pb^{II}, the ^{31}P resonances observed in $_{p}SYG_{ox}$ coalesce and relocate to chemical shifts of −0.43 ppm. These chemical shifts indicate the column force between Pb^{II} ions and the phosphate groups within $_{p}SYG_{ox}$, resulting in the formation of the Pb^{II}-$_{p}SYG_{ox}$ complex. Additionally, we compared the meta-binding capabilities of phosphomelanin ($_{p}SYG_{ox}$) with its counterparts, including natural eumelanin (eumelanin from *Sepia officinalis*), artificial melanin and SYG_{ox} (Fig. 3h and Supplementary Fig. 21). These melanins were incubated with a mixture of HMs (Cr^{II} 468.0 mg L^{-1}, Pb^{II} 84.0 mg L^{-1}, Mn^{II} 660.0 mg L^{-1}, Li^{I} 17.0 mg L^{-1}, Cd^{II} 3.2 mg L^{-1}, Ni^{II} 181.0 mg L^{-1}, Zn^{II} 147.0 mg L^{-1}, Cu^{II} 99.0 mg L^{-1}) that simulated the pollution levels typically encountered in Northeast Asia[51,52]. Upon ICP-OES analysis, phosphomelanin exhibited greater binding efficiencies for Cr^{II}, Mn^{II}, Zn^{II}, Pb^{II} and Cd^{II}, particularly in capturing Li^{I} ions, which is unattainable by other melanins. Phosphomelanin does not demonstrate significant binding advantages for Ni^{II} and Cu^{II} when compared to its counterparts (Fig. 3i and Supplementary Table 2). This observation can be explained by the fact that natural melanins, including *Sepia* eumelanin and artificial melanin, contain catechol functional groups that are capable of forming specific coordination interactions with valence-variable metal ions. These interactions substantially enhance binding capacity and may competitively interfere with phosphate groups-mediated metal ion binding processes[53].

In situ biosynthesis of phosphomelanin in microbes enabling resistance to HMs

We selected two representative microbes as the microbial chassis: a Gram-negative platform strain (*E. coli* TOP 10) and a Gram-positive platform strain (*B. subtilis* 168) to construct an engineered microbial platform capable of biosynthesizing phosphomelanin endogenously. We confirmed that phosphomelanin can be produced across different microbial genera, thereby enabling them to withstand harsh HM conditions.

Initially, we successfully constructed an engineered bacteria (GE-*E. coli*) based on the typical Gram-negative platform strain (*E. coli* TOP 10), capable of heterologous expression of bmTYR (Fig. 4a and Supplementary Fig. 22). We synthesized the bmTYR gene and placed it under the control of the strong constitutive promoter (J23100)[54]. Then, we transformed the recombinant plasmid pUC57-bmTYR into the *E. coli*, resulting in high levels of TYR expression. Following a 12-hour incubation with the substrate $_{p}$SYG, the color of the engineered bacteria (GE-*E. coli*) solution progressively intensified. By combining biochemical methods and cryo-TEM, we confirmed that the phosphomelanin is located both on the cell wall and in the cytoplasm (Fig. 4a and Supplementary Fig. 23). The engineered microbes capable of biosynthesizing phosphomelanin can effectively bind to HMs. This was confirmed through analysis using

https://doi.org/10.1038/s41467-025-60117-5

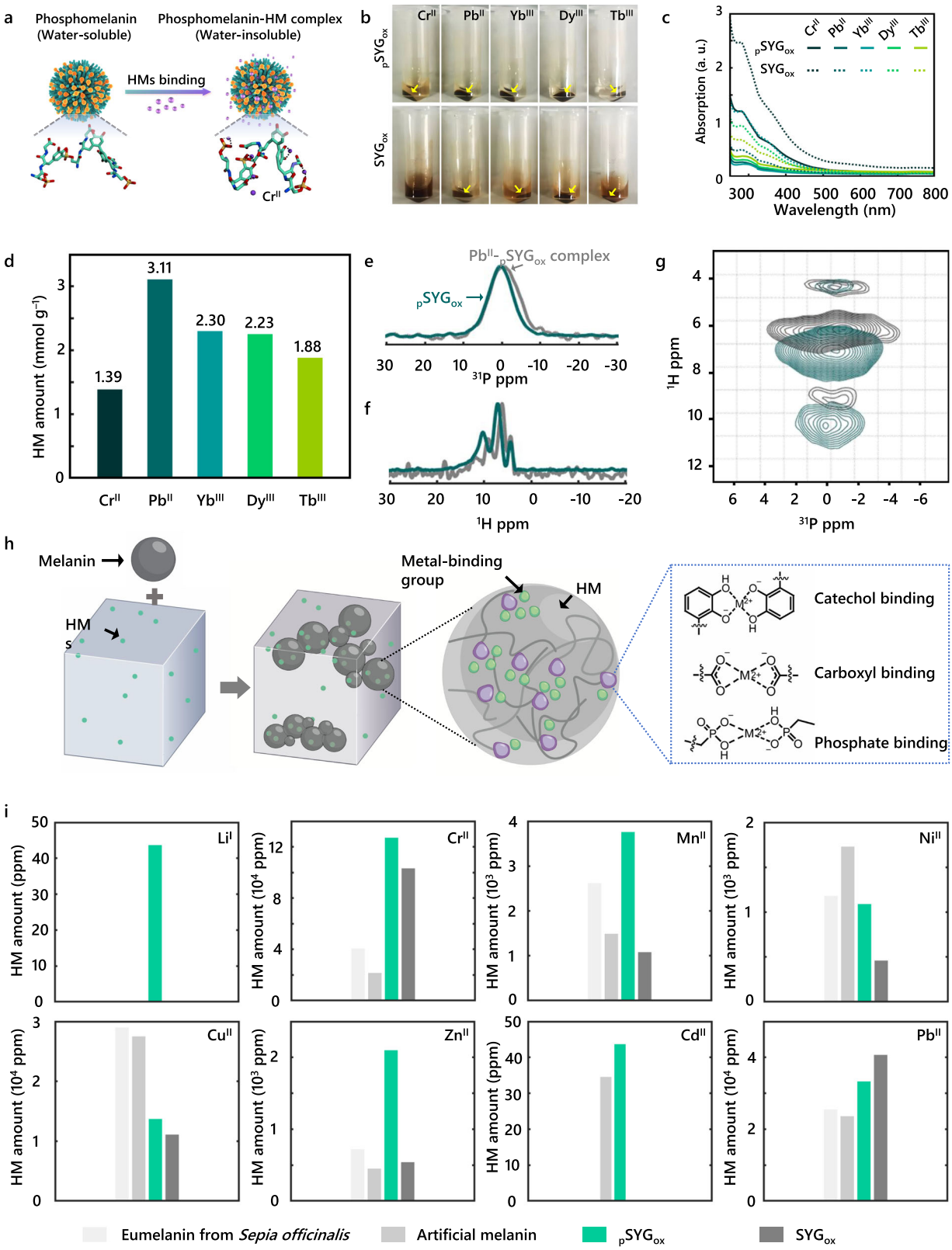

Energy-dispersive X-ray spectroscopy (EDS) and XPS (Fig. 4b and Supplementary Fig. 24).

We compared the surface zeta potentials of WT bacteria (*E. coli*), bacteria that produce phosphorus-free melanin SYG_{ox} (GE-*E. coli* + SYG_{ox}), and bacteria that produce phosphomelanin $_pSYG_{ox}$ (GE-*E. coli* + $_pSYG_{ox}$). The results showed that the GE-*E. coli* bacteria producing phosphomelanin exhibited a more negative charge than *E. coli* alone (−32.23 mV vs. −25.88 mV), which can be attributed to the auto-ionization of phosphorus-containing groups in phosphomelanin around the membrane environment. The GE-*E. coli* producing SYG_{ox} exhibited a less negative charge than *E. coli* alone, which can be attributed to the shielding effect of SYG_{ox} melanin on the bacterial surface charge. This also indirectly confirmed the distribution of melanin on the cell membrane (Fig. 4c). The three microbial strains

Fig. 3 | Metal-binding ability of phosphomelanin. a Schematic representation of the interaction between phosphomelanin, a soluble substance, with HMs. Upon binding with HMs, phosphomelanin forms insoluble complexes. This process results in the sequestration and removal of HMs from the environment. The insert is a scheme of phosphomelanin (left) and simulated phosphomelanin-Cr^{II} complex (right). **b** Visual comparison of the precipitates obtained after mixing melanin ($_pSYG_{ox}$ and SYG_{ox}) solutions with different types of HMs, where the yellow arrow denotes the phosphomelanin-HM complex. Results show that phosphomelanin binds more extensively with HMs than the phosphorus-free melanin, leading to increased precipitate formation and a subsequently clearer supernatant. **c** UV-vis spectra of the supernatants. **d** Quantitative analysis of HMs captured by $_pSYG_{ox}$ using ICP-OES. The (**e**) ^{31}P ssNMR spectra, (**f**) ^{1}H ssNMR spectra, and (**g**) 2D ^{1}H-^{31}P HETCOR spectra of the Pb^{II}-$_pSYG_{ox}$ complex and the metal-free $_pSYG_{ox}$, respectively. These chemical shifts indicate the column forces between Pb^{II} ions and the phosphate group within $_pSYG_{ox}$, resulting in the formation of the Pb^{II}-$_pSYG_{ox}$ complex. **h** Schematic diagram of melanin-metal binding in solution state. **i** Quantitative analysis of HMs captured by different melanins (eumelanin from *Sepia officinalis*, artificial melanin, $_pSYG_{ox}$ and SYG_{ox}) from mixed HM solutions by using ICP-OES ($n = 3$). 1 ppm (parts per million) indicates that 1 μg of metal ions is present per 1 g of the complex. Source data are provided as a Source Data file.

were exposed to seven toxic-level HMs, including Co^{II}, Cr^{II}, Dy^{III}, Mn^{II}, Pb^{II}, Tb^{III}, and Yb^{III}, to evaluate their resistance to toxic-level HMs (Fig. 4d). The bacterial survival under toxic-level HMs was quantified using a colony forming unit (CFU)-based assay[55]. Notably, the engineered *E. coli* containing $_pSYG_{ox}$ demonstrated superior resistance to all tested HMs. In comparison, the engineered *E. coli* containing phosphorus-free melanin (SYG_{ox}) exhibited moderate HM resistance, with poor survival at equivalent concentrations of Co^{II}, Mn^{II}, Pb^{II}, and Tb^{III}, and marked growth suppression in Cr^{II}, Dy^{III} and Yb^{III}. The WT *E. coli* controls showed no observable survival under tested HM conditions.

Besides, ICP-OES was used to assess the HMs-binding ability of these bacterial cells. Compared to the other groups, the engineered bacteria producing phosphomelanin showed enhanced binding capacities for Cr^{2+} and Zn^{2+} (Supplementary Fig. 25). It is worth noting that when we re-inoculated these phosphomelanin-producing engineered microbes, which had bound HMs, into a fresh culture medium and subjected them to shaking incubation, we observed that all these microbes grew vigorously and were capable of continuous division and proliferation. The SEM results show that the engineered microbes maintained intact morphology, uniform size, and clear surface features (Fig. 4e). The above experimental results confirm that, compared with their naturally corresponding microorganisms, engineered microorganisms producing phosphomelanin exhibit higher metal-binding affinity and more advanced protective functions against HMs[56].

By constructing another recombinant shuttle plasmid (pP43-bmTYR), the bmTYR gene can also be successfully expressed in Gram-positive platform strain *B. subtilis* 168. This indicates that the engineering of microbes to produce phosphomelanin is not only achievable in the Gram-negative bacteria but is also feasible across the Gram-positive bacteria (Fig. 4f). Following co-incubation with the substrate $_pSYG$, the engineered bacteria (GE-*B. subtilis*) exhibited significant production of deep-black phosphomelanin. This was further validated by cryo-TEM imaging equipped with EDS, which depicted the deposition of aggregates on the bacterial surface with a distinct contrast to the bacteria themselves (Fig. 4g). ICP-OES measurement and elemental mapping confirmed the presence of phosphorus within these melanin-based aggregates (Fig. 4g, h). Collectively, these findings confirm the biosynthesis of phosphomelanin by the engineered *B. subtilis*. These engineered *B. subtilis* bacteria, which produced phosphomelanin, also exhibited more robust growth under conditions with toxic-level concentrations of HMs, including Cr^{II}, Mn^{II}, Pb^{II}, Tb^{III}, Dy^{III}, Yb^{III} and Co^{II}, compared to bacteria producing phosphorus-free melanin (Fig. 4i).

Due to the steric hindrance between enzymes and substrates[57], microbes containing TYR exhibit lower catalytic efficiency compared to pure TYR, which directly interacts with substrates to catalyze oxidation reactions. However, unmodified or unprotected pure TYR is highly sensitive to environmental HMs. These HMs can inhibit TYR's catalytic activity through copper ion displacement, disruption of protein structure, or oxidative damage[30]. Microbial systems provide protective advantages for TYR through HM isolation and enzyme immobilization mechanisms[58]. Notably, through the refactoring of the phosphomelanin biosynthesis pathway, engineered microbial strains with high TYR expression can achieve resistance to high concentrations of HMs in heavily polluted conditions. This straightforward enzymatic biosynthesis route is distinct from the complex gene regulatory mechanisms[35]. It serves as a simple protective mechanism that not only enables microbes to thrive in extremely harsh HM environments but also facilitates the management of HMs. Synthetic biology, with a sophisticated arsenal of tools, presents an exciting avenue for the creation of a comprehensive microbial platform that produces phosphomelanin in situ a compound with significant potential in neutralizing HM hazards[19].

Phosphomelanin-producing microbes in situ secreted hydrolase for PET depolymerization in HM surroundings

Plastics, particularly microplastics (MPs), when associated with HMs, have emerged as a new class of pollutants. This association can modify the environmental behaviors, bioavailability, and toxicity of the HMs, posing significant ecological risks. However, to date, attention has primarily been focused on the enzymatic degradation of plastic pollutants, with the impact of HMs being largely overlooked[59]. We designed engineered microbes that are capable of producing phosphomelanin and possess plastic-degrading abilities. These engineered microbes can biocatalytically synthesize phosphomelanin, survive in harsh HM environments, bind and resist with HMs. Additionally, they are able to degrade the plastic-HM complex pollutants commonly found in landfill sites for domestic waste and heavy industrial waste. Specifically, we evaluated the degradation of commercial plastic films by engineered bacteria based on the classic soil microorganism *B. subtilis* under these HM-challenging conditions.

Based on the aforementioned research on the genetic engineering of microorganisms, we have further designed a gene cluster with the aim of simultaneously achieving the biodegradation of PET plastic and the adsorption of HMs. This integrated approach could potentially offer a more efficient and targeted solution for environmental remediation, particularly for the treatment of plastic-HMs composite pollutants (Fig. 5a). Here, *B. subtilis* 168 was chosen as a platform to exogenous express recombinant PET hydrolase (PETase). A biosynthetic gene cluster was constructed within a shuttle plasmid pP43-NMK. And then, a constitutive promoter, P43 promoter, was contained within this shuttle plasmid to achieve a non-induced expression. Furthermore, the *Bacillus* signal peptide fragment (SP_{amy}) was fused to the N-terminus of PETase gene from *Indeonella sakainesis* to maximize the excellualr secretion of PETase[60–63]. Simultaneously, the bmTYR gene was also integrated to facilitate the intracellular biosynthesis of phosphomelanin. WB measurements confirmed that PETase was secreted into the extracellular environment, while bmTYR remained within the engineered bacteria (Supplementary Fig. 26). The PETase and bmTYR encoding genes are each preceded by the *B. subtilis* mntA ribosomal binding site (RBS) (AAGAGGAGG), which is a considered as a strong Shine-Dalgarno sequence ($\Delta G > 50.4$ kJ mol^{-1}), to ensure efficient translation[64].

Additionally, the formation of phosphomelanin in engineered bacteria and their HM resistance to Co^{II} and Mn^{II} were demonstrated by

https://doi.org/10.1038/s41467-025-60117-5

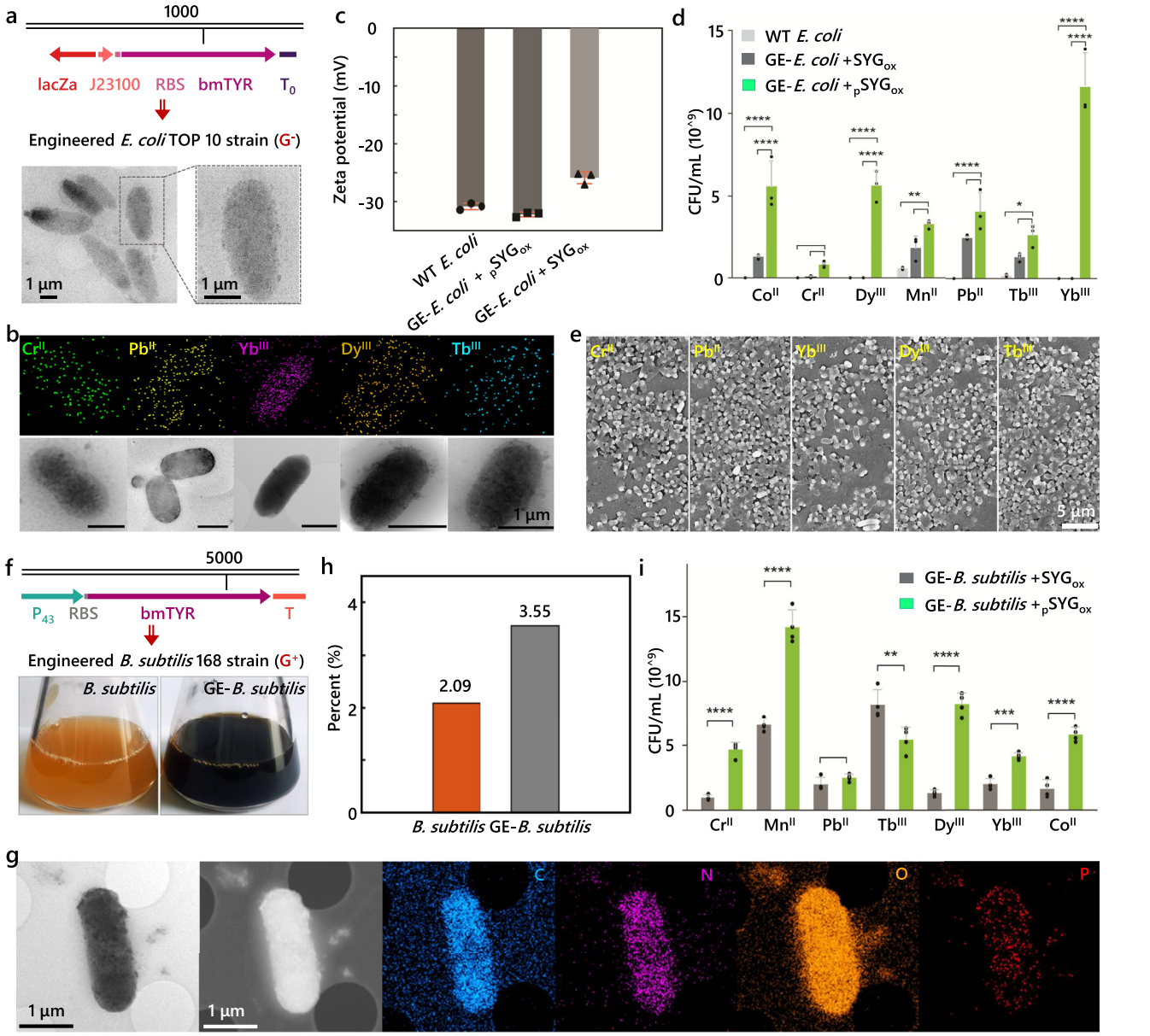

Fig. 4 | In situ biosynthesis of phosphomelanin in microbes enabling resistance to HMs. a The physical map of expression plasmid pUC-bmTYR (upper) and the cryo-TEM images of the engineered *E.coli* TOP 10 strain that has biosynthesized phosphomelanin (below). **b** The EDS images of engineered *E. coli* that was cultured within LB media containing various of HMs. **c** Zeta potentials of bacteria, including WT *E. coli*, GE-*E. coli* containing SYG_{ox}, GE-*E. coli* containing $_pSYG_{ox}$. Data are presented as mean ± SD ($n = 3$, representing three experimental repetitions). **d** The normalized values (CFU/mL) of these bacteria after they had been co-incubated with various HMs. Data presented as mean ± SD ($n = 3$,representing three experimental repetitions). **e** SEM images of the engineered bacteria which had bound HMs, exhibiting healthy appearance. **f** The physical map of expression plasmid pP43NMK-bmTYR (upper) and image of *B. subtilis* and GE-*B. subtilis* after a 24 h incubation with $_pSYG$. The results indicate that the melanin biosynthesis has occurred within the engineered bacteria (below). **g** The cryo-TEM and EDS images of the GE-*B. subtilis* that was cultured within $_pSYG$-containing LB media. **h** ICP-OES analysis of both the *B. subtilis* and GE-*B. subtilis* after a 24-hour co-incubation with the substrate $_pSYG$. The results indicated an approximately 1.7-fold increase in phosphorus content within the GE-*B. subtilis* compared to the *B. subtilis*, with percentages at 3.55% and 2.09%, respectively. **i** The normalized values (CFU/mL) of the GE-*B. subtilis* ($_pSYG$ as the substrate) and GE-*B. subtilis* (SYG as the substrate). These bacteria were co-cultured in LB media, which contained toxic-level concentrations of HMs. Data presented as mean ± SD ($n = 4$, representing four experimental repetitions). Bars represent mean ± SD; ordinary one-way ANOVA. $^*P \le 0.05$; $^{**}P \le 0.01$; $^{***}P \le 0.001$; $^{****}P \le 0.0001$. Source data are provided as a Source Data file.

cyro-TEM, EDS and selected area electron diffraction (SAED) analyses (Fig. 5b and Supplementary Fig. 27). Selecting the monomer of PET, bis (2-hydroxyethyl) terephthalate (BHET) as a model, the biodegradation capability of engineered bacteria in the presence of HMs was further evaluated. As shown in Fig. 5c, these PETase secreted by the engineered bacteria catalyzed in vitro hydrolysis reactions of ester bonds within BHET. The high-resolution ESI-MS measurements confirmed that these ester bonds of BHET were hydrolyzed into terephthalic acid (TPA) and ethylene glycol (EG) monomers (Supplementary Fig. 28). The BHET block degraded into fragments within 1 h and was further digested into smaller pieces after 6 h. Over a period of 36 h, the BHET block was completely decomposed, resulting in a visible clear solution. While there were no morphological changes observed, when the BHET block was inciubated with 50 mM Gly-NaOH buffer (Fig. 5d). The PET film can also be degraded by the engineered bacteria. We immersed BHET blocks and PET films in a solution of engineered bacteria and

https://doi.org/10.1038/s41467-025-60117-5

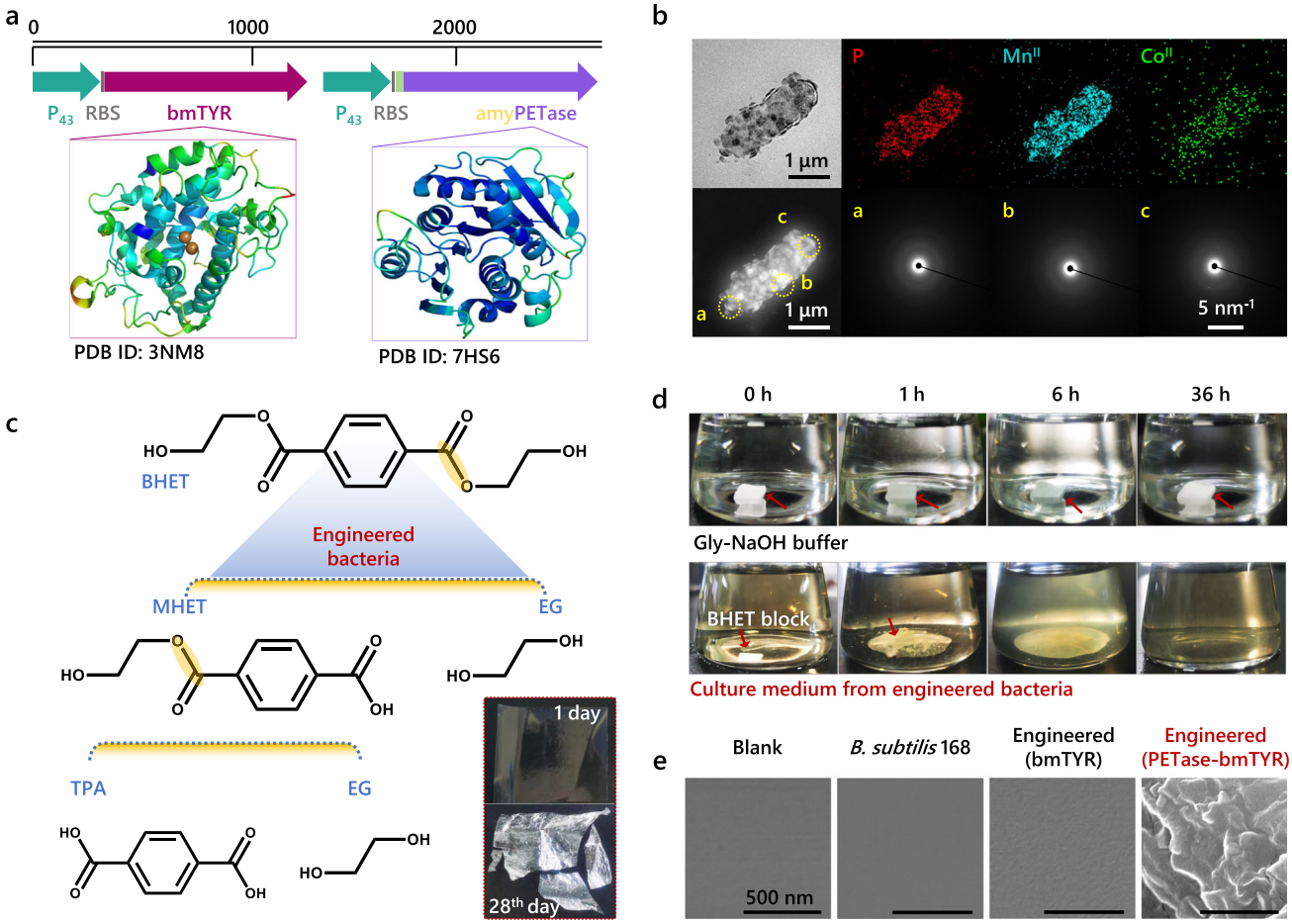

Fig. 5 | The construction of an engineered microbial platform for integrated management of metalized plastic waste. a The physical map depicts the gene clusters designed for the co-expression of both PETase and bmTYR. The inserted figure display the 3D structure images of PETase (Protein Data Bank ID: 7HS6) and abTYR (Protein Data Bank ID: 3NM8). **b** The cyro-TEM, EDS, and SAED images of engineered *B. subtilis* 168 cultured in LB media containing Co^{II} and Mn^{II} (the concentration of HM is 500 mg L^{-1}). The EDS analysis indicated that these HMs were bonded to phosphorus-containing groups within the bacteria. The SAED images showed that these HMs were not present in the form of inorganic phosphate salts. Collectively, these results confirm that the HMs were trapped by organic phosphorus-containing groups derived from phosphomelanin. **c** Schematic diagram of the BHET hydrolysis reaction catalyzed by recombinant PETase secreted by engineered bacteria. The inserted figures display the time-dependent degradation of a commercial PET film by the engineered *B. subtilis* 168. **d** The BHET block, measuring 1.0 × 1.5 × 0.3 cm, underwent hydrolysis in both a 50 mM glycine-NaOH buffer (pH 9.0) and the culture medium of engineered bacteria. The temperature for the hydrolysis was maintained at 50 °C. **e** SEM images of PET films treated with culture medium, *B. subtilis* 168, bmTYR-expressing engineered bacteria, and PETase-bmTYR-expressing engineered bacteria.

assessed their weight loss at various time points to confirm the biodegradation capability of the engineered bacteria on plastics (Supplementary Fig. 29). We can observe that by the 28th day, the intact PET film had been broken down into smaller fragments (Fig. 5c insert). After that, SEM was employed to visually confirm the changes in surface morphology during the PET film degradation process (Fig. 5e). The surface of PET film remained smooth and even when incubated in a culture medium or co-incubated with non-engineered bacteria. However, when incubated with the bmTYR-expressing *B. subtilis* 168 strain, the PET film's surface lost its original luster, attributing to the generation of phosphomelanin. Notably, incubation of the PET film with the engineered PETase-bmTYR-expressing *B. subtilis* 168, resulted in a visibly roughened and wrinkled film surface, indicating the biodegradation of the PET film by the engineered bacteria. This rough surface exposed more reactive sites for PET hydrolysis reactions and sped the whole degeneration course eventually. Moreover, 2D XRD measurements confirmed changes in the crystallographic orientation of the PET film as the degeneration progressed (Supplementary Fig. 30). The PET film exhibited three distinct intensity peaks, where the in-plane crystallographic orientations were represented by peaks with d-spacings of 6.8 Å and 3.9 Å, and the out-of-plane orientation was indicated by a peak with a d-spacing of 3.4 Å. The results showed a decrease in all three crystallographic orientations during the engineered bacteria-induced degeneration, with the out-of-plane orientation (d = 3.4 Å) demonstrating a more pronounced reduction compared to the in-plane orientations (d = 6.8 Å and d = 3.9 Å). This suggests that the PET polymer films, which are packed perpendicularly to the film plane, are more readily catalyzed by PETase secreted by engineered bacteria.

The recombinant PETase enzyme exhibits its highest catalytic activity at approximately 50 °C. However, the chassis microbe *B. subtilis* 168 does not thrive at this high temperature[65]. To address this, we have further developed a thermophilic engineered bacteria based on the *B. subtilis* HT50 (Supplementary Fig. 31). As anticipated, this engineered thermophilic bacteria is not only capable of in situ biosynthesis of phosphomelanin within the bacteria, which effectively binds to HMs such as Co^{II} and Mn^{II}, but also demonstrate excellent biodegradation efficiency for PET at approximately 50 °C. This engineered thermophilic bacteria shows potential as a suitable candidate for industrial strains, where a moderate increase in temperature can enhance the

efficiency of industrial processes for treating plastic-HM composites. In summary, applying principles of synthetic biology (Supplementary Table 3), we have constructed an engineered bacterial platform that offers functionality: it utilizes in situ biosynthesized phosphomelanin for resistance against HMs and also employs the release of PETase enzyme for plastic degradation. The establishment of this engineered bacterial platform provides an efficient and sustainable solution for the treatment of plastic-HM composite pollutants.

Discussion

We have customized and optimized engineered microbial systems that confer resistance against heavy metals and metalized plastic wastes via phosphomelanin biosynthesis, employing biological synthetic methodologies. We have demonstrated that TYR expression in engineered melanogenic microbe is proficient to produce a melanin enriched with phosphorus, which we have designated as phosphomelanin, using a phosphorylated tripeptide as the substrate. We have further delineated the chemical architecture of phosphomelanin, inferring the critical presence of two distinct phosphorus-containing chemical forms: the phosphate monoester group linked to Ser and the phosphate diester group bridging Ser and Tyr. These endogenously biosynthesized phosphomelanins within engineered microbe serve a pivotal role; they exhibit excellent metal-binding capabilities, thereby enhancing the engineered microbes' resistance and tolerance to HMs. Furthermore, we have upgraded these engineered microbes by integrating PET-degrading enzymes, thereby conferring upon them with the dual capabilities of endogenous phosphomelanin biosynthesis and extracellular secretion of PET hydrolases, successfully achieving the biodegradation of metallized plastic waste. These findings underscore the vast potential of engineered microbes capable of producing phosphomelanin, extending their applications far beyond traditional bioremediation. The phosphomelanin, as a member of the melanin family, endows these microbes with an unprecedented opportunity to function effectively in extreme situations, which is poised to foster significant advancements in sustainable manufacturing processes. Moreover, it enables a more holistic and comprehensive approach to the management and treatment of the environmental waste.

Methods

Plasmids and chassis microbes

The plasmid (pUC57-bmTYR, Supplementary Data 1) and the *E. coli* TOP 10 were purchased from Tsingke Biotechnology. The *B. megaterium* (WH320), the *B. subtilis* 168, and the shuttle plasmids (phis 1525-bmTYR, pP43 NMK-bmTYR, pP43 NMK-amyPETase-bmTYR, pHT304) were purchased from Forhigh Biotechnology. The *B. subtilis* HT 50 was isolated from the sewer pipe of the lab. Sequences including DNA sequence of bmTYR for *E. coli*, DNA sequence of bmTYR for *B. megaterium* and *B. subtilis*, DNA sequence of *Indeonella sakainesis* PETase for *B. subtilis*, amino acid sequence of bmTYR and amino acid sequence of *I. sakainesis* PETase were provided in Supplementary Data 2.

Media and reagents

Peptides were purchased from GL Biochem Ltd (Shanghai, China). The ^{1}H NMR and ^{13}C NMR data of the peptides were provided in Supplementary Note 1–8.The abTYR was purchased from Sigma-Aldrich Co., Ltd. (Darmstadt, Germany). LB, TB, and LA cultural media were purchased from Solarbio Science & Technology Co., Ltd. (Beijing, China). Eumelanin from *Sepia Officinalis* was purchased from Xi'an Lyna Biotech., Ltd. (Xi'an, China). Artificial melanin is purchased from Shanghai Macklin Biochemical Technology Co., Ltd. (Shanghai, China). The 6x-His tag monoclonal antibody (4E3D10H2/E3) is purchased from Thermo Fisher Scientific (USA). Additional reagents, including D(+)-xylose, tetracycline, and kanamycin sulfate, were purchased from Solarbio Science & Technology Co., Ltd. (Beijing, China). BHET and dialysis tubes (D-Tube Dialyzer Maxi) were purchased from Sigma-Aldrich Co., Ltd. (Darmstadt, Germany). PET films with a thickness of 0.0125 mm were purchased from DuPont (France). All other chemicals were purchased from Beijing Chemical Co. Ltd. (Beijing, China) and were used without further purification or modification.

Preparation and purification of melanin analogues

Enzymatic oxidation to produce melanin analogues was performed using abTYR and bmTYR under aerobic conditions. Briefly, the TYR-containing precursors ($_{p}$YYG, $_{p}$TYG, $_{p}$SYG, and SYG) were dissolved in PBS (0.1 M, pH 8.5) to a concentration of 5.0 mg mL^{-1} in 10 mL quartz tubes. These tubes were then equipped with polytetrafluoroethylene stoppers and stoppers were sealed with parafilm to ensure airtight conditions. The solutions were saturated with pure oxygen for 30 min to create an oxygen-rich environment. Following saturation, TYR at a concentration of 1.0 KU mL^{-1} was added to the above solutions. The tubes were incubated at room temperature for 24 h with continuous oxygen saturation to facilitate the enzymatic reaction and promote the formation of melanin analogues. To obtain bmTYR, first, the engineered *E. coli* TOP10 were harvested by centrifuging at 3000 × *g* for 3 min at room temperature. The precipitate was remixed and broken under ultrasonic conditions. Next, the lysate was clarified by centrifugation at 20,000 *g* for 30 min at 4 °C and subsequently passed through a 0.45 μm filter. The filtered lysate was purified by Ni-NTA resin and desalinized by desalting column. The product was further analyzed by SDS-PAGE and BCA Protein Assay. Following the enzymatic reactions, the melanin analogues were purified using a size-exclusion chromatography column packed with Bio-Gel P gels (G2, Extra Fine). The column was operated at a flow rate of 0.05 mL min^{-1} with MilliQ water as the mobile phase. The flow rate of the mobile phase was controlled by gravity. The purified melanin analogues ($_{p}$YYG$_{ox}$, $_{p}$TYG$_{ox}$, $_{p}$SYG$_{ox}$, and SYG$_{ox}$) were then sealed individually into dialysis tubes with a molecular weight cut-off of 3.5 kDa. These tubes were immersed in 5 liters of MilliQ water for 48 h to eliminate inorganic phosphates from the PBS. The water was refreshed six times during this period.

In vitro Metal-binding study

Melanin analogues were lyophilized over 48 h. Subsequently, all melanin analogues were redissolved in MilliQ water to a final concentration of 10.0 mg mL^{-1} for both SYG$_{ox}$, and $_{p}$SYG$_{ox}$. Solutions of these melanin analogues (100 μL at 10.0 mg mL^{-1}) were mixed with 900 μL of various metal nitrate solutions (Cr, Pb, Yb, Dy, and Tb at a concentration of 0.5 mmol mL^{-1}). The resulting insoluble metal-binding complexes were obtained by high-speed centrifugation at 15,000 × *g* for 30 min. The complexes were then dialyzed against MilliQ water to remove any free metal ions. For the dialysis process, the insoluble complexes were dispersed in 1.0 mL of MilliQ water, and the samples were sealed in dialysis tubes with a molecular weight cut-off of 3.5 kDa. The tubes were immersed in 1.0 L of MilliQ water for 48 h, with the water being replaced six times over this period.

Characterization of microbial resistance to high HM concentrations

Bacterial samples were derived from single colonies isolated on LB agar plates. Primary cultures were established by inoculating monoclonal clones into 4.0 mL of heavy metal-free LB medium for 12 h. Fresh media supplemented with 20 μM Cu^{2+} (activating enzyme) and equimolar concentrations (1.0 mg mL^{-1} SYG and 1.2 mg mL^{-1} $_{p}$SYG) of peptide powders were inoculated with the primary culture, followed by 24 h incubation. Subsequently, 40 μL aliquots were transferred into 4.0 mL of fresh medium containing the following HM concentrations: Cr (3.75 mM), Pb (5 mM), Yb (4 mM), Dy (6.2 mM), Tb (3.3 mM), Mn (10.6 mM), Co (0.8 mM). After 24 h incubation at 37 °C, serial dilutions of bacterial suspensions were plated on agar. Viable cell counts were

determined using a colony-forming unit (CFU)-based quantification method[55] after an additional overnight incubation at 37 °C. All experimental conditions were tested in triplicate biological replicates.

Morphology characterization

SEM images were captured using a Hitachi S-4800 SEM, with samples placed on the silicon slices. To enhance sample conductivity, a layer of platinum (Pt) was sputtered onto them. Cryo-TEM images were obtained using a JEOL JEM-2310 and F200 instrument. EDS images were obtained using a JEOL JEM-2100F and F200 instrument at a temperature of 100 K, with samples protected by a thin layer of amorphous ice. Zeta potential measurements were conducted using a Malvern Zetasizer Nano ZS ZEN3600. Micrographs were captured using a charge-coupled device (CCD) camera from Gantega, integrated with Olympus Soft Imaging Solutions.

Spectroscopy characterization

FTIR spectra were recorded using a TENSOR-27 infrared spectrometer. 1D ^{1}H, ^{13}C, ^{31}P, and 2D in situ ^{1}H-^{1}H COSY NMR spectra were obtained on a 700-MHz Bruker Avance spectrometer equipped with a triple resonance cryogenic probe and utilizing built-in 1D and 2D pulse sequences. 1D ^{13}C, 1D ^{31}P, and 2D in situ ^{1}H-^{31}P HETCOR ssNMR spectra were obtained using a Bruker AVANCE III 600. The spectrometer is equipped with a magic angle spinning (MAS) 4.0 mm probe. All chemical shifts were referenced to adamantane (δ_H = 1.91 ppm, δ_C = 38.48 ppm). Compressed air was used to regulate the sample's temperature at room temperature. High-resolution ESI-MS were recorded by Fourier transform ion cyclotron resonance mass spectrometry (FT-ICR) using a Bruker Solarix. MALDI-MS were acquired on a Bruker Autoflex III-MALDI-TOF-MS. Each sample for MS characterization was prepared by dissolving the compound into aqueous media in a concentration of approximately 100 μg mL^{-1}. UV-vis absorption spectra were collected using a Shimadzu UV-2600 spectrophotometer with a 1.0 mm pathlength quartz cuvette. Fluorescence measurements were performed using a Hitachi Model FL-4500 spectrofluorometer with a 1.0 cm quartz cuvette. Fluorescence decay measurements were conducted on an Edinburgh FLS1000 steady-state and transient fluorescence spectrometer. EPR measurements at 9.37 GHz were conducted using a Bruker EMXplus-9.5/12 with a microwave power of 20 mW, and all samples were analyzed at 100 K under aerobic conditions. XPS measurements were measured by ESCALab250Xi. ICP values were obtained using a Thermo Scientific iCAP RQ ICP-MS, with all samples requiring lyophilization for 48 h prior to analysis.

Construction of heterogeneous TYR-expressing *E. coli*

The prokaryotic TYR gene from *B. megaterium* (bmTYR) was inserted into the relaxed plasmid pUC57-kan. These plasmids were then introduced into the *E. coli* TOP 10 to express bmTYR. A constitutive promoter, J23100, was utilized to ensure overexpression of bmTYR within Gram-negative bacteria. Subsequently, AGE was performed to verify the correctness of the target sequence in the plasmids. Upon digestion with XbaI and PstI, two electrophoretic bands were observed, located between 800 to 1200 bp and 2000 to 3000 bp, respectively. These results were consistent with the predicted sizes of 1104 bp and 2547 bp.

Construction of endogenous TYR-expressing *B. megaterium*

The endogenous bmTYR was inserted into the shuttle plasmid phis1525, which is capable of transferring between the *E. coli* TOP 10 and the *B. megaterium* WH320. The transformation protocol for *B. megaterium* WH320 follows established methodologies[66,67]. In brief, the cells were grown in LB medium at 37 °C to mid-log phase ($OD_{600} \approx 0.5$), then chilled on ice and harvested by centrifugation at 4 °C. For each transformation, 50 μL of electrocompetent cells were mixed with 1-2 μg of plasmid DNA and transferred to a pre-chilled 0.2 cm electroporation cuvette. Electroporation was performed at 2.5 kV, 25 μF, and 200 Ω. Immediately after pulsing, 1.0 mL of pre-warmed SOC medium was added, and cells were incubated at 37 °C with shaking for 1-2 h before plating on a tetracycline-containing LB agar. The plasmid phis1525 includes the promoter and repressor gene from the *B. megaterium* operon responsible for xylose utilization. Expression of bmTYR is inducible by xylose, with 0.5% xylose added to the culture medium to induce expression; non-inducing broth contains no xylose. All media for culturing the *B. megaterium* WH320 are supplemented with tetracycline at a concentration of 20 μg mL^{-1}.

Construction of heterogeneous TYR-expressing *B. subtilis*

The bmTYR was inserted in the shuttle plasmid pP43 NMK[68,69]. This recombinant plasmid was then introduced into the *B. subtilis* 168 to express bmTYR. The constitutive promoter P43 was utilized to ensure the overexpression of bmTYR within the gram-positive bacteria[70].

Construction of heterogeneous bi-enzyme-expressing *B. subtilis*

The bmTYR, the PETase gene from *Ideonella sakaiensis*, and the signal peptide (*amy*) gene from *Bacillus amyloliquefaciens* were inserted into the shuttle plasmid pP43-NMK-kan. The recombinant plasmids were then introduced into the *B. subtilis* to enable the co-expression of bmTYR and the secretion of PETase. For the *B. subtilis* HT 50, the three genes were inserted into the shuttle plasmid pHT304. Electroporation was employed to transform all these plasmids into the bacteria.

Western blot analysis

Total bacterial protein from *B. megaterium* and *B. subtilis* was extracted using the BestBio bacterial total protein extraction kit. Protein quantification was performed using the BestBio BCA protein quantification kit. A cell lysate containing 30 mg of WH320 was mixed with Laemmli buffer (Bio-Rad) containing 5% 2-mercaptoethanol and boiled at 95 °C for sample preparation. SDS-PAGE was conducted using 15 mL, 15-well precast mini-PROTEAN TGX gels (Bio-Rad) in a Mini-PROTEAN tetra cell at 200 V with 1 × Tris/glycine/SDS running buffer (Bio-Rad). A PageRuler Plus pre-stained protein ladder (Thermo Fisher) was used as a molecular weight marker. Proteins were then transferred onto Immobilon-FL PVDF membranes (Millipore Sigma) at 100 V for 1 h at 4 °C using 1× Tris/glycine transfer buffer (Bio-Rad) with 0.2% methanol. Membranes were blocked at room temperature for 1 h with Odyssey blocking buffer (TBS, LI-COR). A monoclonal anti-6x his-tag antibody (ThermoFisher, 4E3D10H2/E3) was used to detect TYR at a dilution of 1:500.

Production of phosphomelanin within the engineered bacteria

The engineered bacteria (*E. coli* TOP 10, *B. megaterium* WH320, or *B. subtilis* 168) were cultured in LB medium. Specifically, a 10 mL overnight culture of engineered bacteria was inoculated into a 200 mL flask with 50 mL of sterile LB. Here, 100 μg mL^{-1} kanamycin was added to the engineered *E. coli* and engineered *B. subtilis* 168, while 20 μg mL^{-1} tetracycline was added to the engineered *B. megaterium* WH320. The engineered bacteria were incubated at 37 °C with shaking at 220 rpm for 24 h. Subsequently, the substrate ($_p$SYG or SYG) was added to the culture media. The engineered bacteria were then broken using ultrasound, and the resulting suspension was centrifuged at 4 °C to separate the components. The dark, clear supernatant was collected and lyophilized eventually. The crude phosphomelanin produced by the engineered bacteria was further purified using a size-exclusion chromatography column with MilliQ water as the mobile phase. Finally, ^{31}P ssNMR measurements were conducted to reveal the structural information of the purified products.

Identification and quantitation of products in BHET or PET degradation in vivo

The optimal reaction buffer for the recombinant PETase is 50 mM glycine-NaOH buffer at pH 9.0, which contains 10% (*v*/*v*) crude enzyme

solution. The enzyme was used to hydrolyze a block of BHET measuring 1.0 × 1.5 × 0.3 cm at 50 °C for 36 h. The hydrolytic products were subsequently analyzed directly using MS.

The engineered *B. subtilis* 168 was cultured in TB medium. Specifically, a 10 mL overnight culture of engineered bacteria was inoculated into a 200 mL flask with 100 mL of sterile LB, 10 μg mL^{-1} kanamycin, 10 μg mL^{-1} $_{p}$SYG, 100 μg mL^{-1} Co^{II}, and 100 μg mL^{-1} Mn^{II} ion. The engineered bacteria were incubated at 37 °C with shaking at 220 rpm for 24 h with the BHET block (100 mg) or PET film (5.0 × 5.0 cm). As for the engineered HT 50, the culture temperature remains at 50 °C.

Molecular docking

A Lamarckian genetic algorithm in AutoDock (Molecular Graphics Laboratory, La Jolla, CA, USA) was applied for the molecular docking study[71,72]. The structural information of abTYR (PDB ID: 5M6B) was retrieved from the Protein Data Bank. The initial conformations of $_{p}$SYG and SYG within the active pocket of abTYR for the docking simulation were determined using density functional theory (DFT) calculations at the B3LYP/6-31 G* level, which were carried out using CP2K (version 2023.1) package[73].

Statistical analysis

The error bars represent the standard error calculated from multiple experimental repetitions, with a minimum of three replicates per experiment, reflecting the variability and reliability of our measurements. Data are presented as mean ± SD. Statistical analysis was performed using ordinary one-way ANOVA. $^{*}P \le 0.05$; $^{**}P \le 0.01$; $^{***}P \le 0.001$; $^{**}P \le 0.0001$. These error bars were generated using MATLAB 2024b and incorporated into the figures to illustrate the variability across replicates.

Reporting summary

Further information on research design is available in the Nature Portfolio Reporting Summary linked to this article.

Data availability

Data supporting the findings of this work are available within the paper and its Supplementary Information files. A reporting summary for this article is available as a Supplementary Information file. Source data are provided with this paper.

References

1. Nriagu, J. O. & Pacyna, J. M. Quantitative assessment of worldwide contamination of air, water and soils by trace metals. *Nature* **333**, 134–139 (1988).
2. White, C., Shaman, A. K. & Gadd, G. M. An integrated microbial process for the bioremediation of soil contaminated with toxic metals. *Nat. Biotechnol.* **16**, 572–575 (1998).
3. Qu, C. C. et al. Heavy metal behaviour at mineral-organo interfaces: mechanisms, modelling and influence factors. *Environ. Int.* **131**, 104995 (2019).
4. Aziz, H. A., Adlan, M. N. & Ariffin, K. S. Heavy metals (Cd, Pb, Zn, Ni, Cu and Cr (III)) removal from water in Malaysia: post treatment by high quality limestone. *Bioresour. Technol.* **99**, 1578–1583 (2008).
5. Krishnan, K. & Plane, R. A. Raman spectra of ethylenediaminetetraacetic acid and its metal complexes. *J. Am. Chem. Soc.* **90**, 3195–3200 (1968).
6. Peruzzini, M., Gonsalvi, L. & Romerosa, A. Coordination chemistry and functionalization of white phosphorus via transition metal complexes. *Chem. Soc. Rev.* **34**, 1038–1047 (2005).
7. Brulle, R. J. & Pellow, D. N. Environmental justice: human health and environmental inequalities. *Annu. Rev. Public Health* **27**, 103–124 (2006).
8. Sun, G. L., Reynolds, E. E. & Belcher, A. M. Using yeast to sustainably remediate and extract heavy metals from waste waters. *Nat. Sustain.* **3**, 303–311 (2020).
9. Hou, D. et al. Metal contamination and bioremediation of agricultural soils for food safety and sustainability. *Nat. Rev. Earth Env.* **1**, 366–381 (2020).
10. Lovley, D. R. & Lloyd, J. R. Microbes with a mettle for bioremediation. *Nat. Biotechnol.* **18**, 600–601 (2000).
11. Sousa, C., Cebolla, A. & de Lorenzo, V. Enhanced metalloadsorption of bacterial cells displaying poly-His peptides. *Nat. Biotechnol.* **14**, 1017–1020 (1996).
12. Li, X. et al. Response of soil microbial communities and microbial interactions to long-term heavy metal contamination. *Environ. Pollut.* **231**, 908–917 (2017).
13. Aljerf, L. & AlMasri, N. A gateway to metal resistance: bacterial response to heavy metal toxicity in the biological environment. *Ann. Adv. Chem.* **2**, 32–44 (2018).
14. Xie, W. J., Dhinojwala, A., Gianneschi, N. C. & Shawkey, M. D. Interactions of melanin with electromagnetic radiation: from fundamentals to applications. *Chem. Rev.* **124**, 7165–7213 (2024).
15. Pavan, M. E., Pavan, E. E., López, N. I., Levin, L. & Pettinari, M. J. Living in an extremely polluted environment: clues from the genome of melanin-producing Aeromonas salmonicida subsp. pectinolytica 34melT. *Appl. Environ. Microbiol.* **81**, 5235–5248 (2015).
16. Tran-Ly, A. N., Ribera, J., Schwarze, F. W., Brunelli, M. & Fortunato, G. Fungal melanin-based electrospun membranes for heavy metal detoxification of water. *SMT* **23**, e00146 (2020).
17. Rajkumar, M., Ma, Y. & Freitas, H. Improvement of Ni phytostabilization by inoculation of Ni resistant *Bacillus megaterium* SR28C. *J. Environ. Manag.* **128**, 973–980 (2013).
18. Nascimento, F. X., Hernández, A. G., Glick, B. R. & Rossi, M. J. Plant growth-promoting activities and genomic analysis of the stress-resistant *Bacillus megaterium* STB1, a bacterium of agricultural and biotechnological interest. *Biotechnol. Rep.* **25**, e00406 (2020).
19. Rusk, N. Engineering wild bacteria. *Nat. Methods* **15**, 764–764 (2018).
20. Walker, K. T. et al. Self-pigmenting textiles grown from cellulose-producing bacteria with engineered tyrosinase expression. *Nat. Biotechnol*. https://doi.org/10.1038/s41587-024-02194-3 (2024).
21. Singh, S. et al. Microbial melanin: Recent advances in biosynthesis, extraction, characterization, and applications. *Biotechnol. Adv.* **53**, 107773 (2021).
22. Martínez, L. M., Martinez, A. & Gosset, G. Production of melanins with recombinant microorganisms. *Front Bioeng. Biotechnol.* **7**, 285 (2019).
23. Choi, K.-Y. Bioprocess of microbial melanin production and isolation. *Front. Bioeng. Biotechnol.* **9**, 765110 (2021).
24. Siwicka, Z. E. et al. Synthetic porous melanin. *J. Am. Chem. Soc.* **143**, 3094–3103 (2021).
25. Horsman, G. P. & Zechel, D. L. Phosphonate biochemistry. *Chem. Rev.* **117**, 5704–5783 (2017).
26. Westheimer, F. H. Why nature chose phosphates. *Science* **235**, 1173–1178 (1987).
27. Chang, R., Yuan, C. Q., Zhou, P., Xing, R. R. & Yan, X. H. Peptide self-assembly: from ordered to disordered. *Acc. Chem. Res.* **57**, 289–301 (2024).
28. Yuan, C. Q. et al. Hierarchically oriented organization in supramolecular peptide crystals. *Nat. Rev. Chem.* **3**, 567–588 (2019).
29. Chang, R., Zhao, L. Y., Xing, R. R., Li, J. B. & Yan, X. Y. Functional chromopeptide nanoarchitectonics: molecular design, self-assembly and biological applications. *Chem. Soc. Rev.* **52**, 2688–2712 (2023).
30. Solomon, E. I., Sundaram, U. M. & Machonkin, T. E. Multicopper oxidases and oxygenases. *Chem. Rev.* **96**, 2563–2606 (1996).

31. Rygus, T. & Hillen, W. Inducible high-level expression of heterologous genes in *Bacillus megaterium* using the regulatory elements of the xylose-utilization operon. *Appl. Microbiol. Biotechnol.* **35**, 594–599 (1991).
32. Obermeyer, A. C., Jarman, J. B. & Francis, M. B. N-terminal modification of proteins with o-aminophenols. *J. Am. Chem. Soc.* **136**, 9572–9579 (2014).
33. Marmelstein, A. M. et al. Tyrosinase-mediated oxidative coupling of tyrosine tags on peptides and proteins. *J. Am. Chem. Soc.* **142**, 5078–5086 (2020).
34. Ren, X. K. et al. The dominant role of oxygen in modulating the chemical evolution pathways of tyrosine in peptides: dityrosine or melanin. *Angew. Chem. Int. Ed.* **58**, 5872–5876 (2019).
35. Ren, X. K. et al. Enzyme-driven oxygen-fuelled pathway selectivity of tyrosine-containing peptide oxidation evolution. *Chem. Eng. J.* **450**, 138293–138293 (2022).
36. Wachter, R. M. Chromogenic cross-link formation in green fluorescent protein. *Acc. Chem. Res.* **40**, 120–127 (2007).
37. Zhou, X. et al. Artificial regulation of state transition for augmenting plant photosynthesis using synthetic light-harvesting polymer materials. *Sci. Adv.* **6**, eabc5237 (2020).
38. Seidel, K. et al. Studying molecular 3D structure and dynamics by high-resolution solid-state NMR: application to L-tyrosine-ethylester. *J. Phys. Chem. A* **109**, 2436–2442 (2005).
39. Laws, D., Bitter, H. & Jerschow, A. Solid-state NMR spectroscopic methods in chemistry. *Angew. Chem. Int. Ed.* **41**, 3096–3129 (2002).
40. Lampel, A. et al. Polymeric peptide pigments with sequence-encoded properties. *Science* **356**, 1064–1068 (2017).
41. Purdela, D. Theory of ^{31}P NMR chemical shifts. II. Bond-angle dependence. *J. Magn. Reson.* **5**, 23–36 (1971).
42. Letcher, J. H. & Van Wazer, J. R. Theoretical Interpretation of ^{31}P NMR chemical shifts. *I. J. Chem. Phys.* **44**, 815–829 (1966).
43. Tang, H. Wang, Y. High-resolution NMR spectroscopy in human metabolism and metabonomics. *In*: Webb, G. A. (*eds*) *Modern Magnetic Resonance*. Springer, Dordrecht (2008).
44. Zhu, Y. et al. Complete biosynthetic pathway of the phosphonate phosphonothrixin: two distinct thiamine diphosphate-dependent enzymes divide the work to form a C–C bond. *J. Am. Chem. Soc.* **144**, 16715–16719 (2022).
45. Shiraishi, T. & Kuzuyama, T. Biosynthetic pathways and enzymes involved in the production of phosphonic acid natural products. *Biosci. Biotechnol. Biochem.* **85**, 42–52 (2021).
46. Fujieda, N. et al. Post-translational his-cys cross-linkage formation in tyrosinase induced by Copper (II)-peroxo species. *J. Am. Chem. Soc.* **133**, 1180–1183 (2011).
47. Pretzler, M., Bijelic, A. & Rompel, A. Heterologous expression and characterization of functional mushroom tyrosinase (AbPPO4). *Sci. Rep.* **7**, 1810 (2017).
48. Daumann, L. J. Essential and ubiquitous: the emergence of lanthanide metallobiochemistry. *Angew. Chem. Int. Ed.* **58**, 12795–12802 (2019).
49. Iuga, A., Ader, C., Gröger, C. & Brunner, E. Applications of solid-state ^{31}P NMR spectroscopy. *Annu. Rep. NMR Spectro.* **60**, 145–189 (2006).
50. Hanrahan, M. P. et al. Enhancing the resolution of ^{1}H and ^{13}C solid-state NMR spectra by reduction of anisotropic bulk magnetic susceptibility broadening. *Phys. Chem. Chem. Phys.* **19**, 28153–28162 (2017).
51. Jeong, H., Choi, J. Y., Lee, J., Lim, J. & Ra, K. Heavy metal pollution by road-deposited sediments and its contribution to total suspended solids in rainfall runoff from intensive industrial areas. *Environ. Pollut.* **265**, 115028 (2020).
52. Cheng, S. Heavy metal pollution in China: origin, pattern and control. *Environ. Sci. Pollut. Res. Int* **10**, 192–198 (2003).
53. Szpoganicz, B., Gidanian, S., Kong, P. & Farmer, P. Metal binding by melanins: studies of colloidal dihydroxyindole-melanin, and its complexation by Cu(II) and Zn(II) ions. *J. Inorg. Biochem.* **89**, 45–53 (2002).
54. Ting, W.-W. et al. Whole-cell biocatalyst for cadaverine production using stable, constitutive and high expression of lysine decarboxylase in recombinant *Escherichia coli* W3110. *Enzym. Microb. Technol.* **148**, 109811 (2021).
55. Franken, N. et al. Clonogenic assay of cells in vitro. *Nat. Protoc.* **1**, 2315–2319 (2006).
56. Kim, Y. J., Wu, W., Chun, S. E., Whitacre, J. F. & Bettinger, C. Catechol-mediated reversible binding of multivalent cations in eumelanin half-cells. *Adv. Mater.* **26**, 6572–6579 (2014).
57. Li, J. et al. Regulation of lanthanide supramolecular nanoreactors via a bimetallic cluster cutting strategy to boost aza-Darzens reactions. *Nat. Commun.* **16**, 2169 (2025).
58. Sheldon, R. A. & van Pelt, S. Enzyme immobilisation in biocatalysis: why, what and how. *Chem. Soc. Rev.* **42**, 6223–6235 (2013).
59. Sullivan, K. P. et al. Mixed plastics waste valorization through tandem chemical oxidation and biological funneling. *Science* **378**, 207–211 (2022).
60. Lu, H. et al. Machine learning-aided engineering of hydrolases for PET depolymerization. *Nature* **604**, 662–667 (2022).
61. Wang, N. et al. Enhancing secretion of polyethylene terephthalate hydrolase PETase in *Bacillus subtilis* WB600 mediated by the SPamy signal peptide. *Lett. Appl. Microbiol.* **71**, 235–241 (2020).
62. Yoshida, S. et al. A bacterium that degrades and assimilates poly (ethylene terephthalate). *Science* **351**, 1196–1199 (2016).
63. Son, H. F. et al. Rational protein engineering of thermo-stable PETase from Ideonella sakaiensis for highly efficient PET degradation. *ACS Catal.* **9**, 3519–3526 (2019).
64. Xue, D. et al. Refactoring and heterologous expression of class III lanthipeptide biosynthetic gene clusters lead to the discovery of N, N-dimethylated lantibiotics from firmicutes. *ACS Chem. Biol.* **18**, 508–517 (2023).
65. Su, F. & Xu, P. Genomic analysis of thermophilic strains: efficient producers for platform bio-chemicals. *Sci. Rep.* **29**, 3926 (2014).
66. Moro, A., Sánchez, J. C. & Serguera, C. Transformation of *Bacillus megaterium* by electroporation. *Biotechnol. Tech.* **9**, 589–590 (1995).
67. Lopes, W. et al. Optimization of a medium composition for the heterologous production of alcaligenes faecalis penicillin G acylase in *Bacillus megaterium*. *Protein Expres Purif.* **210**, 106327 (2023).
68. Zhang, X. et al. Modular pathway engineering of key carbon-precursor supply-pathways for improved N-acetylneuraminic acid production in *Bacillus subtilis*. *Biotechnol. Bioeng.* **115**, 2217–2231 (2018).
69. Zhang, A. L., Liu, H., Yang, M. M., Gong, Y. S. & Chen, H. Assay and characterization of a strong promoter element from *B. subtilis*. *Biochem. Biophys. Res. Commun.* **354**, 90–95 (2007).
70. Jiang, Z. et al. Secretory expression fine-tuning and directed evolution of diacetylchitobiose deacetylase by *Bacillus subtilis*. *Appl. Environ. Microbiol.* **85**, e01076–01019 (2019).
71. Forli, S. et al. Computational protein-ligand docking and virtual drug screening with the AutoDock suite. *Nat. Protoc.* **11**, 905–919 (2016).
72. Morris, G. M. et al. AutoDock4 and AutoDockTools4: Automated docking with selective receptor flexibility. *J. Comput. Chem.* **30**, 2785–2791 (2009).
73. Kühne, T. D. et al. CP2K: An electronic structure and molecular dynamics software package-Quickstep: Efficient and accurate electronic structure calculations. *J. Chem. Phys.* **152**, 194103 (2020).

Acknowledgements
We are grateful to Dr. Zonglin Liang from the Institute of Microbiology, Chinese Academy of Sciences and Forhigh Biotechnology for their insightful discussions, which greatly assisted in the design of the TYR-expressing system. We also extend our thanks to Dr. Junfeng Xiang at the Center for Analysis and Measurement, Institute of Chemistry, Chinese Academy of Sciences for his valuable input on the design of the NMR measurements. This work was financially supported by the National Key R&D Program of China (Nos. 2023YFC3404200, 2023YFC3404202 to X.Y., L.Z. and R.X.), the National Natural Science Foundation of China (Nos. 22025207 to X.Y., 22377127 to R.X., 52361145848 to R.X., 22477121 to L.Z.), the Beijing Nova Program (Nos. 20230484352, 20240484650 to R.X.), the progress of Strategy Priority Research Program (Category B) of Chinese Academy of Sciences (No. XDB0520301 to R.X.), and the IPE Project for Frontier Basic Research (Grant No. QYJC-2023-05 R.X.).

Author contributions
X.Y., R.X. and X.R. conceived the idea and designed the experiments. X.R., L.Z., J.S. carried out the sample preparation, purification and characterization. L.Z., C.Y. assisted with the chemical analysis of MS and NMR measurements. L.Z. and P.Z. contributed to the MD simulations and kinetic analysis. K.Z. contributed to PET degeneration experiment, film structural characterization and data analysis. X.R., R.X. and X.Y. wrote the paper with inputs from all authors.

Competing interests
The authors declare no competing interests.

Additional information
Supplementary information The online version contains supplementary material available at https://doi.org/10.1038/s41467-025-60117-5.

Correspondence and requests for materials should be addressed to Ruirui Xing or Xuehai Yan.

Peer review information *Nature Communications* thanks the anonymous reviewers for their contribution to the peer review of this work. A peer review file is available.